Optical and Quantum Electronics **24** *(1992) S927–S949*

Determination of laser beam parameters with the phase space beam analyser

N. HODGSON, T. HAASE
Festkörper-Laser-Institut Berlin GmbH, Strasse des 17. Juni 135, D-1000 Berlin 12, Germany

R. KOSTKA, H. WEBER
Optisches Institut, Technische Universität Berlin Strasse des 17.Juni 135, D-1000 Berlin 12, Germany

Received 16 January; accepted 24 April 1992

The properties of the phase space beam analyser (PSBA), first introduced by Nemes, were investigated theoretically and experimentally. This optical system enables one to measure far-field divergence and beam radius of a laser beam simultaneously. Experiments were performed with a pulsed Nd : YAG laser with stable and unstable resonators and with a HeNe laser in fundamental mode operation. The theoretical description was based on Fresnel integrals, which were solved numerically using a FFT algorithm. The results presented indicate that the PSBA provides a simple means to determine beam quality and to investigate the mode properties of optical resonators, if diffraction effects are properly compensated.

1. Introduction

In many areas of laser application where small focus diameter and large Rayleigh ranges are required, the beam quality plays an important role. The parameter which specifies the beam quality is defined by the beam parameter product $d\theta/4$, where d denotes the beam waist diameter and θ is the full angle of divergence (Fig. 1). The beam parameter product relates the focal spot area F to the Rayleigh range z_0, the distance at which the beam cross-section has increased by a factor of 2. For circular symmetry the relation is

$$d\theta/4 = F/z_0 \tag{1}$$

According to the ISO standard, d and θ are defined by the 86.5% energy content, which for

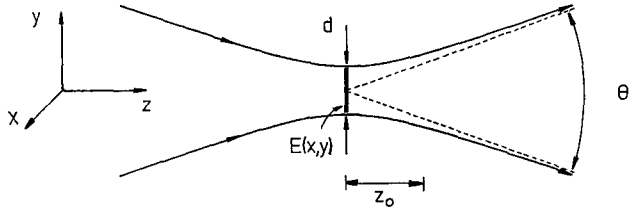

Figure 1 The beam quality of a laser beam is determined by the beam parameter product $d\theta/4$ which relates the focal spot size to the Rayleigh range z_0.

0306–8919

a Gaussian beam means that these quantities coincide with the values given by the $1/e^2$ intensity decrease. Unfortunately, for non-Gaussian field distributions calculation or measurement of d and θ does not give the beam radius at any distance from the waist, since no propagation rules in terms of geometrical optics exist.

Such a rule can be found if beam radius $d/2$ and divergence $\theta/2$ are defined by the second moments of the corresponding intensity distributions [2, 3]. In one dimension they are given by

$$\langle d^2/4\rangle = 4\int_{-\infty}^{\infty} I(x)x^2\,\mathrm{d}x \Big/ \int_{-\infty}^{\infty} I(x)\,\mathrm{d}x \tag{2}$$

$$\langle \theta^2/4\rangle = 4\int_{-\infty}^{\infty} I_F(\Phi)\Phi^2\,\mathrm{d}\Phi \Big/ \int_{-\infty}^{\infty} I_F(\Phi)\,\mathrm{d}\Phi \tag{3}$$

with $I(x)$ the intensity distribution in the waist, $I_F(\Phi)$ the far-field intensity distribution, and Φ the angle of divergence. With these definitions of waist diameter and far-field angle the beam diameter $\langle d(z)^2\rangle$ at any distance z from waist can be calculated with the generalized $ABCD$ law [3]:

$$\langle d(z)^2\rangle = A^2\langle d^2\rangle + B^2\langle\theta^2\rangle \tag{4}$$

where A and B denote the upper elements of the ray matrix. Unfortunately, no fixed relation between this beam diameter and the energy content exists, so that this definition is of academic interest only. Furthermore, the second moment does not exist for intensity distributions which decrease slower than $1/x^2$, like the far-field of a homogeneously illuminated slit.

It is for this reason that the definition of diameter by 86.5% energy enclosure is used to determine the beam quality. From the theoretical point of view this means that the field distribution $E(x, y)$ in the waist and its Fourier transform $F(E(x, y))$ must be known. Beam radius $d/2$ and far-field angle $\theta/2$ in one dimension can then be calculated by

$$\int_{-d/2}^{d/2} |E(x, 0)|^2\,\mathrm{d}x = 0.865\int_{-\infty}^{\infty} |E(x, 0)|^2\,\mathrm{d}x \tag{5}$$

$$\int_{-\theta/2}^{\theta/2} |F(E(x, 0))|^2\,\mathrm{d}\Phi = 0.865\int_{-\infty}^{\infty} |F(E(x, 0))|^2\,\mathrm{d}\Phi \tag{6}$$

In order to get the beam diameter at a distance z from the waist, the field must first be propagated by means of Fresnel integrals before Equation 5 can be applied.

It is obvious that the experimental determination in general requires two measurements: the recording of the intensity distributions in the near- and far-fields. The common way to accomplish this is to produce a waist behind a focusing lens, and after recording the intensity distribution the corresponding Fourier transform is measured in the focal plane of a second lens. This technique, of course, requires sufficient constancy of the beam properties during measurement. Apart from this problem, the procedure is time-consuming especially if the dependence of the beam parameter product on the resonator properties – like refractive power in solid state lasers – has to be determined.

Any optical system capable of measuring the beam parameter product in one step would therefore be very advantageous. The phase space beam analyser (PSBA) [1, 6] has this ability to determine beam quality with a single measurement, but in one dimension only. This is of course no restriction, as long as beams with circular or rectangular symmetry are considered. Otherwise two measurements have to be performed.

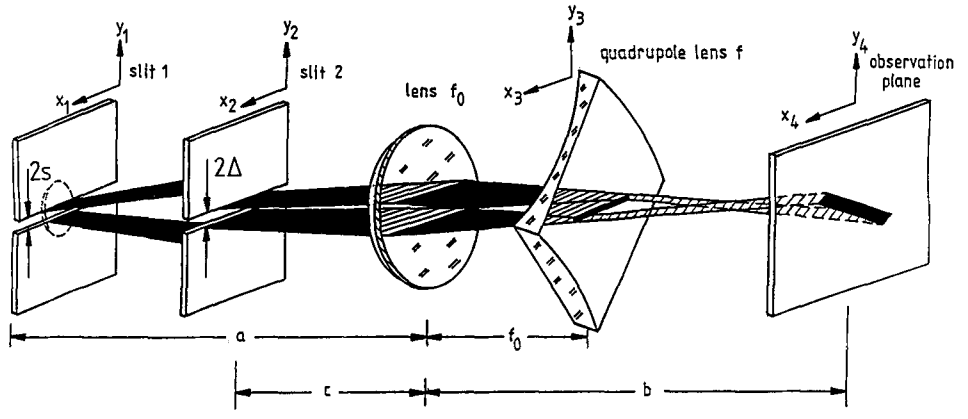

Figure 2 Set-up of the PSBA. A one-dimensional light distribution with respect to size and angle of divergence is produced by the two slits.

2. Geometrical description

The set-up of the PSBA is shown in Fig. 2. At slit 1 the incident field $E_1(x_1, y_1)$ is reduced to a one-dimensional distribution $E_1(x_1, 0)$. Without the quadrupole lens f the image of this line source appears in the observation plane, since the lens equation

$$1/a + 1/b = 1/f_0 \tag{7}$$

holds for the distances a, b and the focal length f_0 of the spherical lens. The quadrupole lens consists of two cylindrical lenses with focal lengths f and $-f$, the focal lines of which are perpendicular to each other.

When the quadrupole lens is inserted with its principal axes rotated by 45° with respect to the x-direction, the circular symmetry of the PSBA is destroyed and simple prediction of the image on plane 4 is not possible. A first understanding can be gained by propagating rays through the system by means of geometrical matrix optics. A more detailed discussion of this treatment can be found in [1, 4, 6]. In the following only the main results are reviewed.

A ray starting at plane 1 is characterized by a four-dimensional vector

$$\boldsymbol{v}_1 = (x_1, y_1, x_1', y_1')$$

where x_1, y_1 are the distances from the optical axis and x_1', y_1' the slopes. The ray arriving in the observation plane is related to the incident ray by a 4 × 4 ray matrix $\boldsymbol{M}_{14}$

$$\boldsymbol{v}_4 = \boldsymbol{M}_{14}\boldsymbol{v}_1 \tag{8}$$

with

$$\boldsymbol{M}_{14} = -\begin{bmatrix} \alpha & 0 & 0 & \beta \\ 0 & \alpha & \beta & 0 \\ 1/f_0 & 0 & 1/\alpha & f_0/f \\ 0 & 1/f_0 & f_0/f & 1/\alpha \end{bmatrix}$$

where Equation 1 has been used with the scaling factors

$$\alpha = (b - f_0)/f_0 \qquad \beta = (f_0/f)(b - f_0) \tag{9}$$

The ray coordinates on plane 4 are thus given by

$$x_4 = -\alpha x_1 - \beta y_1' \tag{10}$$

$$y_4 = -\beta x_1' - \alpha y_1 \tag{11}$$

Since the first slit is assumed to be infinitesimally small, y_1 can be set to zero. The second slit, which we choose to be located at the spherical lens, absorbs all rays with slopes larger than Δ/a. In geometrical optics, this slit can be chosen arbitrarily thin, since diffraction effects are not taken into account. For small slit widths $2s$ and 2Δ, Equations 10 and 11 are

$$x_4 = -\alpha x_1 \qquad y_4 = -\beta x_1' \tag{12}$$

In the observation plane the phase space representation of the incident line source is observed, scaled by the factors α and β. A light source characterized by its size Δx_1 and its angle range $\Delta x_1'$ will produce an illuminated area $\alpha\beta\,\Delta x_1\,\Delta x_1'$ on plane 4 from which the beam parameter product $\Delta x_1\,\Delta x_1'$ can be determined.

Figure 3 shows calculated patterns produced by the intersection points of the rays arriving in plane 4 for a one-dimensional light source whose number of rays $W(x, x')\,dx\,dx'$ starting on plane 1 per area $dx\,dx'$ is given by the Wigner–Wolf function:

$$W(x, x') = \text{const.} \times \exp\left[-\frac{x^2}{2w^2} - \left(\frac{2\pi}{\lambda}\right)^2 \left(\frac{-x}{2R} + x'\right)^2 \frac{w^2}{2} \right]$$

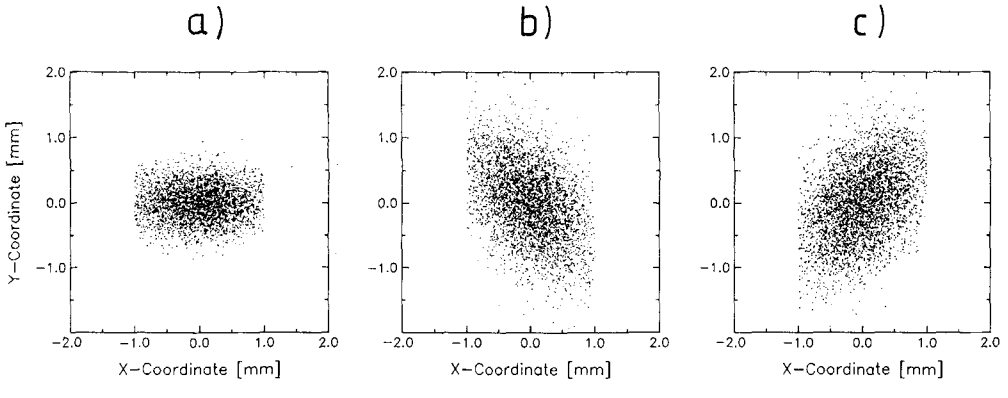

Figure 3 Intersection points of rays on the observation plane of a PSBA calculated with Equation 12 (a = 140 mm, b = 350 mm, f_0 = 100 mm, f = 25 mm). The line source on plane 1 has a Gaussian spatial intensity distribution (number of rays per unit length) with beam radius w = 0.2 mm and an angular intensity distribution given by the Wigner–Wolf function. In these three pictures the radius of curvature R in this geometric Gaussian beam model was changed. (a) $R = \infty$, (b) $R = -2z_0$, (c) $R = 2z_0$ with $z_0 = \pi w_0^2/\lambda$ being the Rayleigh range.

It is known [4, 5] that this is a very useful approach for describing geometrically the beam propagation of a Gaussian beam with beam radius w and radius of curvature R. The rotation of the ellipse in the observation plane with changing radius of curvature R of the field on plane 1 is in agreement with the experimental observation, as will be shown later.

In reality the intensity distribution on plane 4 will of course be affected by diffraction from slit 2 and will therefore be superposed by the phase space distribution of a homogeneously illuminated slit. In order to determine the beam parameter product of the incident beam correctly, it is necessary to take account of this. In the following the beam propagation inside the PSBA is described by means of Fresnel integrals.

3. Diffraction theory

The propagation of the incident field distribution $E_1(x_1, y_1)$ to the planes 2, 3 and 4 can easily be performed by common two-dimensional Fresnel integrals [7, 8], taking into account the phase shift $\Phi(x, y)$ of the rotated quadrupole lens:

$$\Phi(x, y) = -(2\pi/f\lambda)xy \tag{13}$$

With the assumption that the second slit is located at the spheical lens ($c = 0$ in Fig. 2), the relations for the field distributions on the three planes are

$$E_2(x_2, y_2) = C_1 \int_{-s}^{s} \int_{-\infty}^{\infty} E_1(x_1, y_1) \times \exp\left[\mathrm{j}\,(\pi/\lambda a)(x_1^2 + x_2^2 + y_1^2 + y_2^2 - 2(x_1x_2 + y_1y_2))\right] \mathrm{d}x_1\,\mathrm{d}y_1 \tag{14}$$

$$E_3(x_3, y_3) = C_2 \exp\left(\mathrm{j}\Phi(x_3, y_3)\right) \int_{-\Delta}^{\Delta} \int_{-\infty}^{\infty} E_2(x_2, y_2) \times \exp\left[\mathrm{j}(\pi/\lambda f_0)(x_3^2 + y_3^2 - 2(x_2x_3 + y_2y_3))\right] \mathrm{d}x_2\,\mathrm{d}y_2 \tag{15}$$

$$E_4(x_4, y_4) = C_3 \int_{-\infty}^{\infty} \int_{-\infty}^{\infty} E_3(x_3, y_3) \times \exp\left\{\mathrm{j}[\pi/\lambda(b - f_0)](x_3^2 + x_4^2 + y_3^2 + y_4^2 - 2(x_3x_4 + y_3y_4))\right\} \mathrm{d}x_3\,\mathrm{d}y_3 \tag{16}$$

where C_1 to C_3 are constants. These integral equations were solved numerically using a FFT algorithm with 512 × 512 points. Figure 4 shows calculated intensity distributions on the four planes for a Gaussian beam with beam radius $w_0 = 0.4$ mm and planar wavefront. Only 64 × 64 of the calculated points are shown in this graph. As already seen in the geometrical calculations, a Gaussian field distribution produces an ellipse in the observation plane, but now additional side lobes appear which are caused by diffraction at the second slit. The angle Φ_A by which the connecting line of the side lobes is rotated with respect to the x-axis depends only on the set-up of the PSBA. The expression for Φ_A is [6]

$$\tan \Phi_A = b/\beta \tag{17}$$

The direction given by the intensity valleys between these side lobes is in general not perpendicular to the direction determined by Φ_A. Depending on the set-up and the q-parameter q_1 of the Gaussian beam on plane 1 they are rotated by an angle Φ_B, which is

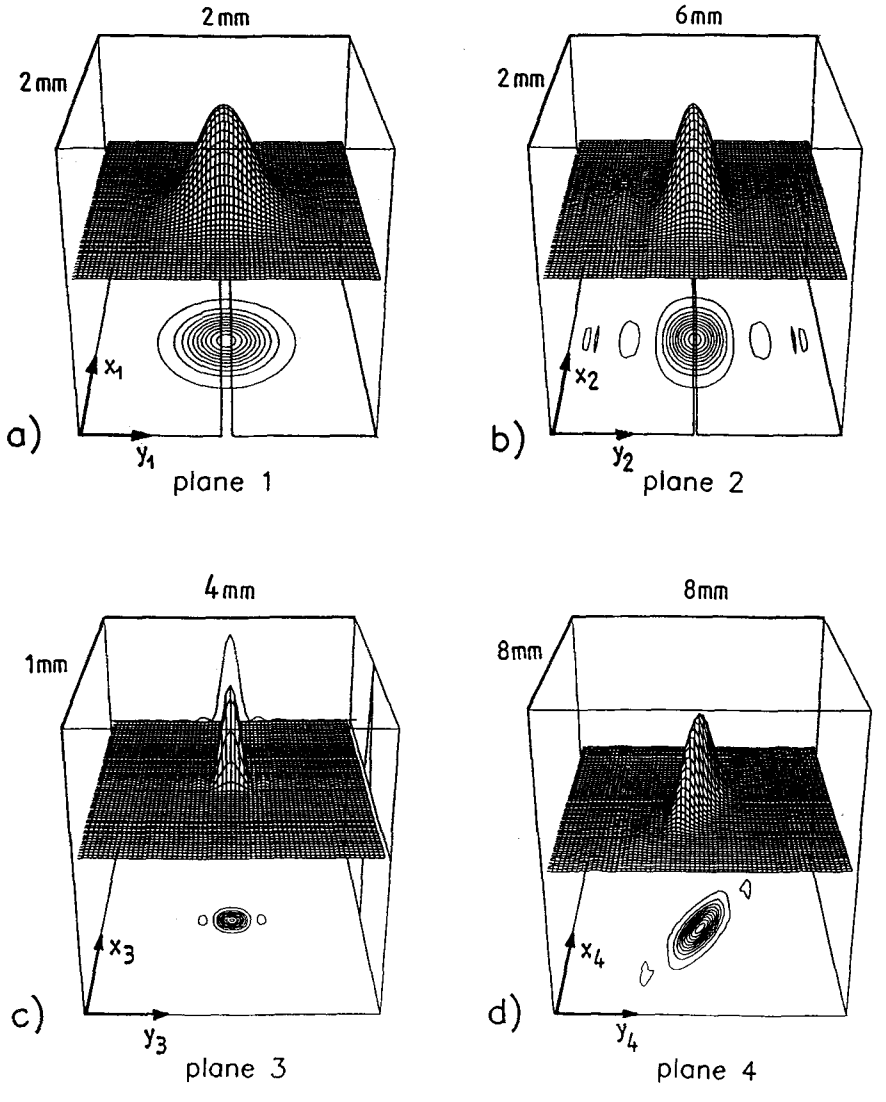

Figure 4 Calculated intensity distributions on the four planes of a PSBA (see Fig. 2) with a = 140 mm, b = 350 mm, c = 0, f_0 = 100 mm, f = 50 mm, s = 40 μm, Δ = 0.1 mm, λ = 0.6328 μm: (a) in front of slit 1, (b) in front of slit 2, (c) on the quadrupole lens, (d) in the observation plane.

given by [6]

$$\tan \Phi_B = -\frac{\beta}{\alpha} \frac{\alpha b/R_1 + \beta^2/|q_1|^2}{\alpha b + \beta^2/R_1} \tag{18}$$

with R_1 the radius of curvature of the Gaussian beam on plane 1.

Some calculated examples of differently rotated intensity patterns in the observation plane for a Gaussian mode are shown in Fig. 5 with the angles given by Equations 17 and 18 indicated as straight lines. Apart from this dependence of the side lobe structure on the beam parameters and the PSBA set-up, an additional rotation of the ellipse can be observed

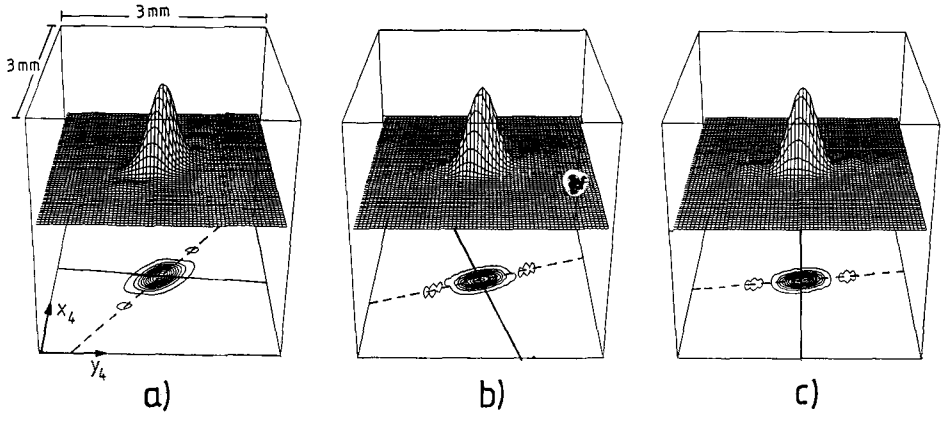

Figure 5 Intensity distributions on the observation plane calculated with Equations 14 to 16 for a Gaussian beam with beam radius $w_0 = 0.5$ mm and planar wavefront (a = 140 mm, $b = 350$ mm, $c = 0$, $f_0 = 100$ mm, $s = 25\,\mu$m, $\Delta = 0.2$ mm, $\lambda = 0.6328\,\mu$m). The angles Φ_A (broken line) and Φ_B (solid line) calculated with Equations 17 and 18 are indictated. (a) $f = 50$ mm, $\Phi_A = 35°$, $\Phi_B = -86°$; (b) $f = 200$ mm, $\Phi_A = 70.3°$, $\Phi_B = -14.6°$; (c) $f = 500$ mm, $\Phi_A = 81.8°$, $\Phi_B = -0.95°$.

which depends on the width 2Δ of slit 2 and the q-parameter q_1 of the incident beam. As will be shown later, this rotation is very useful in tracking any change of mode structure in phase space, because the orientation of the ellipse strongly depends on the phase distribution in plane 1. The derivation of the expression for this rotation angle Φ_C can again be found in [6].

The same relations still hold if higher-order modes are considered. The orientation of the resulting profile in the observation plane is the same as for a Gaussian mode. This is shown in Fig. 6 for Gauss–Laguerre modes of different radial order P and azimuthal order $l = 0$. The widths of the resulting profile are now enlarged in both directions, according to the increased beam radius and divergence of the incident distributions which are plotted on the left-hand side. It is obvious from this figure that a relation between beam radius and divergence in planes 1 and 4 of the PSBA exists. First it is of course necessary to define beam radius $(d/2)_{PSBA}$ and an angle of divergence $(\theta/2)_{PSBA}$ in the observation plane. According to Equations 5 and 6, a useful definition is given by

$$\int_{-\alpha(d/2)_{PSBA}}^{\alpha(d/2)_{PSBA}} \int_{-\infty}^{\infty} |E_4(x_4, y_4)|^2 \, dy_4 \, dx_4 = 0.865 \int_{-\infty}^{\infty} \int_{-\infty}^{\infty} |E_4(x_4, y_4)|^2 \, dy_4 \, dx_4 \qquad (19)$$

$$\int_{-\beta(\theta/2)_{PSBA}}^{\beta(\theta/2)_{PSBA}} \int_{-\infty}^{\infty} |E_4(x_4, y_4)|^2 \, dx_4 \, dy_4 = 0.865 \int_{-\infty}^{\infty} \int_{-\infty}^{\infty} |E_4(x_4, y_4)|^2 \, dx_4 \, dy_4 \qquad (20)$$

These sizes must be compared with those determined from Equations 5 and 6 for the incident field distribution $E_1(x_1, 0)$.

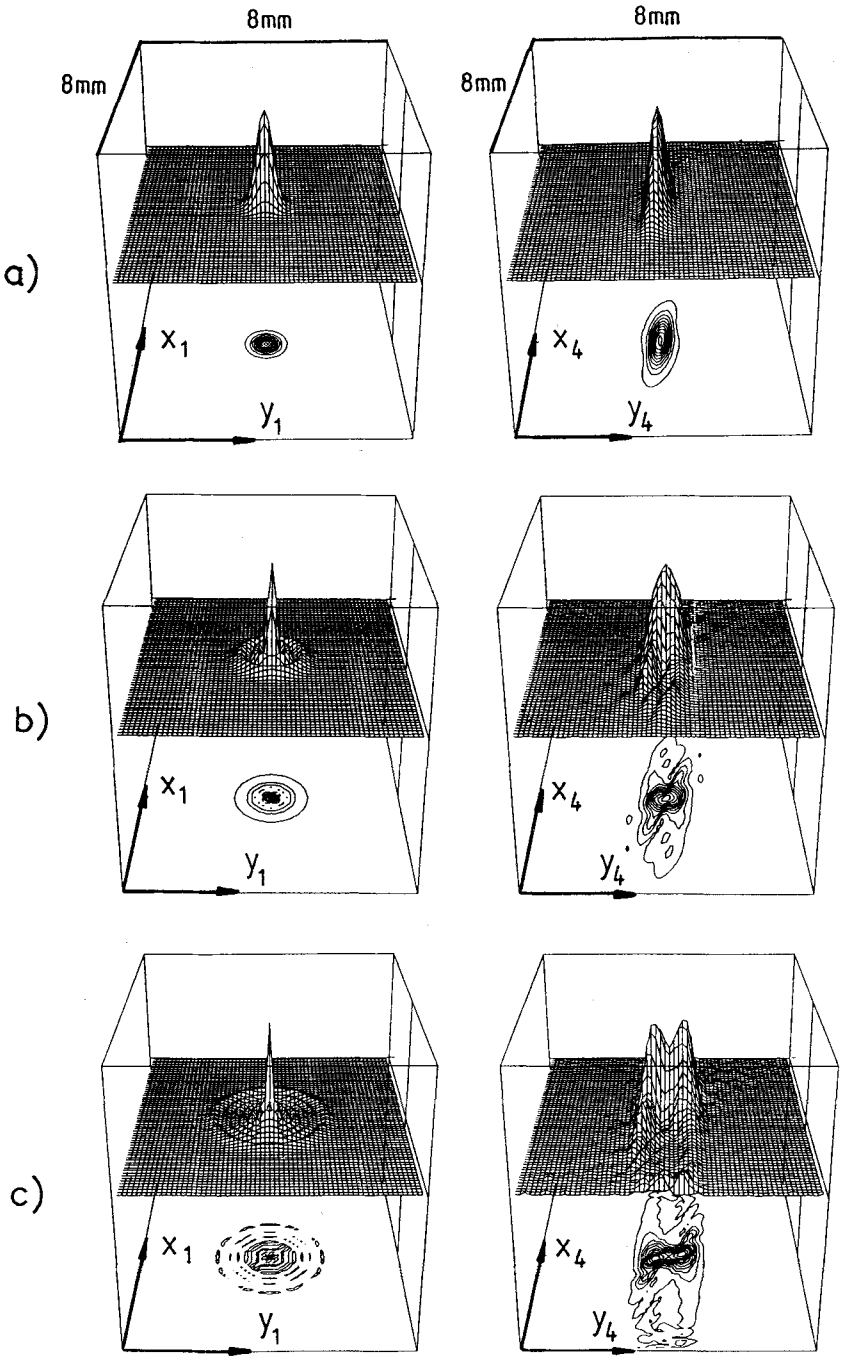

Figure 6 Calculated intensity distributions in the observation plane (right-hand diagrams) of a PSBA for Gauss–Laguerre modes with Gaussian beam radius w_0 = 0.5 mm and different radial orders (a = 140 mm, b = 350 mm, f_0 = 100 mm, f = 50 mm, s = 20 μm, Δ = 0.2 mm, λ = 0.6328 μm). The left-hand diagrams represent the corresponding input intensity distributions at the entrance slit of the PSBA. The radial order is p = 0 at the top, p = 2 in the middle and p = 6 at the bottom.

4. Theoretical results

Two PSBAs were chosen for the theoretical investigation showing different spatial and angular resolution. These two PSBAs are denoted in the following as PSBA 1 (a = 140 mm, b = 350 mm, f_0 = 100 mm, f = 50 mm, α = 2.5, β = 500 mm) and PSBA 2 (a = 242.8 mm, b = 170 mm, f_0 = 100 m, f = 200 mm, α = 0.7, β = 35 mm). In order to investigate the dependence of $(d/2)_{\mathrm{PSBA}}$ and $(\theta/2)_{\mathrm{PSBA}}$ on the incident beam properties, Equations 14–16 and Equations 19 and 20 were solved numerically using Gauss–Hermite modes $E_m(x)$ as incident fields with

$$E_m(x) = \exp(-x^2/w_0^2) H_m(\sqrt{2}x/w_0) \tag{21}$$

with H_m Hermite-polynomial of order m and w_0: beam radius of fundamental mode $E_0(x)$. The results for m = 0 to 4 are presented in Fig. 7 as a function of the width 2Δ of slit 2. In these pictures slit 1 was chosen to be s = 25 μm. Changing s to 15 μm or 50 μm, however, did not affect the results at all. The broken lines indicate beam radius $d/2$ and angle of divergence $\theta/2$ of the incident field, calculated using Equations 5 and 6. It is obvious that the values that can be measured with the PSBA are always enlarged by diffraction at slit 2. In order to get more insight in this behaviour it is advantageous to look at the propagation of the second moments through the PSBA. A propagation rule similar to Equation 4 can be found using four-dimensional ray matrices [9]. The final expression is [6]

$$\langle x_4^2 \rangle = \alpha^2(\langle d^2/4 \rangle + (\beta^2/b^2)\langle y_s^2 \rangle + (f_0^4/f^2)\langle \theta_s^2 \rangle) \tag{22}$$

$$\langle y_4^2 \rangle = \beta^2(\langle \theta^2/4 \rangle + (b^2/\beta^2)\langle \theta_s^2 \rangle) \tag{23}$$

Although these relations hold only for apodized slits, they indicate that the diffraction at slit 2 influences the measured beam radii and angles of divergences by the second moments $\langle y_s^2 \rangle$ of the slit transmission function and by the second moment $\langle \theta_s^2 \rangle$ of the corresponding far field distribution. Unfortunately, these expressions are not valid if the 86.5% energy content is considered. Nevertheless, it is worth applying Equations 22 and 23 to the 86.5% energy definition of beam radius and divergence. Using the corresponding values $y_s = 0.865\Delta$ and $\theta_s = 0.566\lambda/\Delta$ for the slit, Equations 22 and 23 are transformed to

$$(d/2)^2_{\mathrm{PSBA}} = \alpha^2\left((d/2)^2 + 0.75(\beta^2/b^2)\Delta^2 + 0.32(f_0^4/f^2)(\lambda/\Delta)^2\right) \tag{24}$$

$$(\theta/2)^2_{\mathrm{PSBA}} = \beta^2\left((\theta/2)^2 + 0.32(b^2/\beta^2)(\lambda/\Delta)^2\right) \tag{25}$$

Figure 8 shows the results if these equations are applied to the two PSBAs using the values $(d/2)$ and $(\theta/2)$ of the previous figure. A comparison of the two figures indicates that these formulae give roughly the correct dependence of $(d/2)_{\mathrm{PSBA}}$ and $(\theta/2)_{\mathrm{PSBA}}$ on the slit width 2Δ. Equations 24 and 25 are thus very useful for optimizing the performance of a PSBA with the ratio b/β as a key parameter. If this ratio is large, the beam radius can be measured exactly as Equation 24 indicates. For a small ratio the additional term in Equation 25 becomes small compared to $(\theta/2)$ and a high resolution for the divergence measurement is obtained. This is in agreement with the rotation angle Φ_A given by Equation 17. For large b/β ($\Phi_A \approx 90°$) the side lobes of the intensity distributions in plane 4 are located in the y-direction and affect the determination of the divergence. Small ratios b/β do not rotate the intensity distribution and the side lobes will therefore only influence the determination of beam radius. This reveals that without correction either the beam radius or the diver-

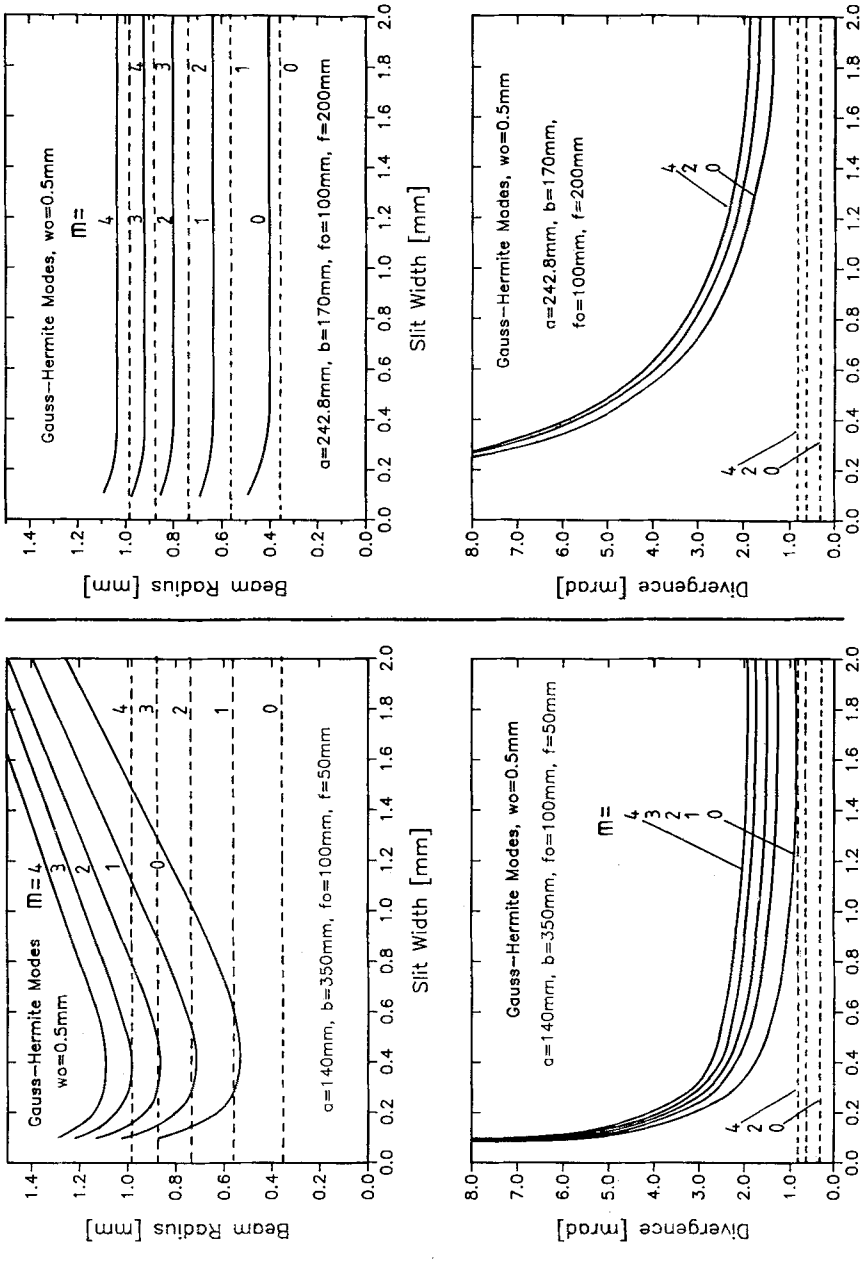

Figure 7 Beam radii $(d/2)_{PSBA}$ and angles of divergence $(\theta/2)_{PSBA}$ of two PSBAs calculated with Equations 14 to 16 and Equations 19 and 20 against the width 2Δ of slit 2. The incident fields are Gauss–Hermite modes of order $m = 0$ to 4 with planar wavefront and Gaussian beam radius $w_0 = 0.5$ mm. The broken lines mark the corresponding input values calculated with Equations 5 and 6. (a) PSBA 1: $a = 140$ mm, $b = 350$ mm, $f_0 = 100$ mm, $f = 50$ mm, $\lambda = 0.6328\,\mu$m, $s = 25\,\mu$m. (b) PSBA 2: $a = 242.8$ mm, $b = 170$ mm, $f_0 = 100$ mm, $f = 200$ mm, $\lambda = 1.064\,\mu$m, $s = 25\,\mu$m.

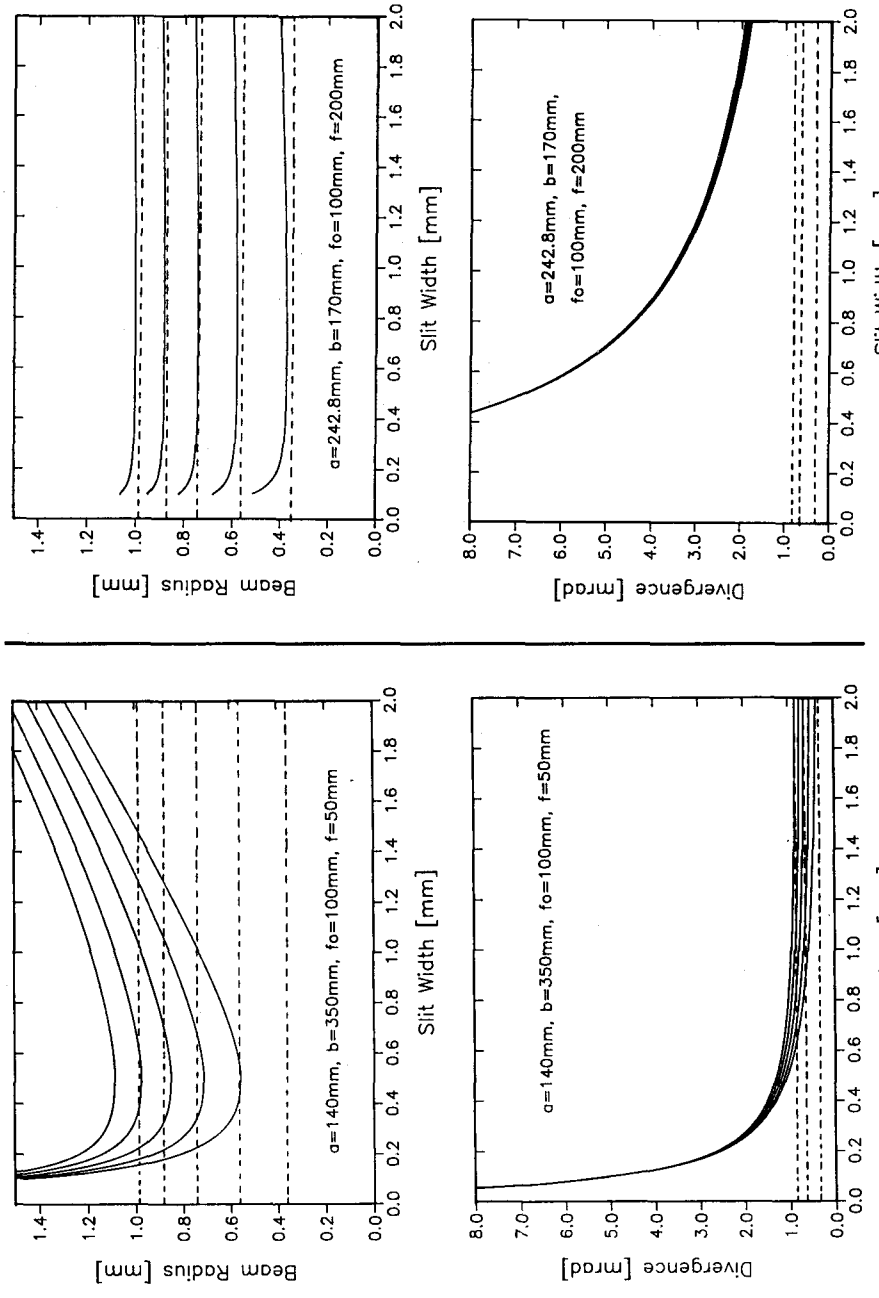

Figure 8 Beam radii $(d/2)_{PSBA}$ and angles of divergence $(\theta/2)_{PSBA}$ for the two PSBAs shown in Fig. 7, calculated with Equations 24 and 25. The beam radius can be predicted well, whereas the quadratic correction formula (25) does not hold for the divergence.

gence can be measured exactly and both measurements become more exact the larger the beam radius and the angle of divergence.

In general, the relations between $(d/2)_{PSBA}$, $(\theta/2)_{PSBA}$ and $(d/2)$, $(\theta/2)$ are more complicated than Equations 24 and 25 predict. We have observed that in addition to the parabolic dependence a shift is present. More useful relations which connect the PSBA-values with the 'real' ones would therefore read

$$(d/2) = \sqrt{[(d/2)^2_{PSBA} - f_1(\Delta)]} - f_2(\Delta) \tag{26}$$

$$(\theta/2) = \sqrt{[(\theta/2)^2_{PSBA} - g_1(\Delta)]} - g_2(\Delta) \tag{27}$$

where f_i and g_i depend on the set-up of the PSBA and on the slit width 2Δ. There are two ways to find these correction functions. They can be determined either by solving the Fresnel integrals (14) to (16) for input fields of different radii and divergences or by calibrating the PSBA experimentally with laser beams of known radius and divergence. For any practical application of the PSBA, the latter method is of course more advantageous, since systematic errors induced by the measurement technique and the set-up of the PSBA are taken into account. We chose this calibration method and determined the functions f_i and g_i with fundamental modes.

5. Experiments

5.1. Set-up

A CCD camera with a sensitive area of $6 \times 8\,mm^2$ and 512×512 pixels was used in connection with an image-processing system to record the intensity distribution in plane 4. The set-up of the PSBA and the maximally detectable beam radii $(d/2)_{max}$ and angles of divergence $(\theta/2)_{max}$ are primarily fixed by the dimensions of the CCD chip. For PSBA 1, laser beams with radii up to 1 mm and divergences up to 3.5 mrad could be detected. We used this set-up for a HeNe laser in TEM_{00} mode operation with the beam waist of $w_0 = 0.313\,mm$ located 7 cm behind the exit aperture. With PSBA 2, much higher radii and divergences could be measured ($(d/2)_{max} \approx 4\,mm$, $(\theta/2)_{max} \approx 60\,mrad$). This system was set up to investigate the beam properties of a pulsed Nd : YAG laser consisting of a 150-mm-long rod of 10 mm diameter and different optical resonators. The rod was pumped by two krypton flashlamps with 3-ms pulse duration and a maximum input power of 12 kW. The refractive power of the rod was determined to be $0.3\,m^{-1}$ per kW of electrical pumping power.

For an optimum performance of the PSBA, it is very important to choose entrance slit 1 as small as possible. Apart from the creation of a line source, this slit must provide a one-dimensional intensity distribution across slit 2, with a homogeneous profile in the y-direction. This means that the Fraunhofer pattern of the slit must appear on slit 2 with a width of the central maximum at least five times larger than the slit width 2Δ. These conditions result in two equations from which s and Δ can be determined:

$$s < \sqrt{[0.01(a - c)\lambda]} \tag{28}$$

$$\Delta < (a - c)\lambda/(10s) \tag{29}$$

These expressions indicate that slit 2 should be located as near as possible to the spherical lens f_0 ($c = 0$). For the two PSBAs used, Equations 28 and 29 yield

PSBA 1 ($\lambda = 0.6328\,\mu m$): $s < 30\,\mu m$, $\Delta < 0.3\,mm$

and

PSBA 2 ($\lambda = 1.064\,\mu$m): $s < 51\,\mu$m, $\Delta < 0.51$ mm

All results presented in this paper were obtained with slit widths of $2s = 50\,\mu$m and $2\Delta < 1.22$ mm. We increased the slit width $2s$ to $100\,\mu$m several times but no effect on the results could be observed, which is in agreement with Equations 28 and 29.

In order to get the beam radius $(d/2)_{\mathrm{PSBA}}$ and divergence $(\theta/2)_{\mathrm{PSBA}}$, the image-processing system was programmed with Equations 19 and 20. Before applying the PSBA, the beam radius $d/2$ and the angle of divergence $\theta/2$ were measured in plane 1 according to Equations 5 and 6.

For both PSBAs the quadrupole lens with focal lens f was formed by a combination of a spherical lens with focal lens $f_s = f$ and a cylindrical lens with focal length $f_c = -f/2$, rotated by 45° with respect to the x-axis. It can easily be verified that these two lenses produce the same phase shift $\Phi(x, y)$ (Equation 13) as two cylindrical lenses with focal lengths f and $-f$. All lenses used in the experiments were made of glass without any antireflecting coating. Interference patterns caused by reflections on the lens surfaces could not be observed. The fringes which can be seen in some of the following photographs are caused by a glass plate glued onto the CCD chip for protection purposes. Their effect on the determination of beam radius and divergence was proved to be negligible.

5.2. Calibration

Both PSBAs were first tested with Gaussian beams of different waist radii w_0 with the waist located on slit 1. The width of slit 1 was chosen to be $50\,\mu$m. The measured beam radii $(d/2)_{\mathrm{PSBA}}$ and divergences $(\theta/2)_{\mathrm{PSBA}}$ versus the slit width 2Δ of slit 2 are shown in Fig. 9 in comparison with the theoretical curves given by Equations 14–16 and 19 and 20. The broken lines again indicate beam radius $d/2$ and $\theta/2$ of the incident field. These figures were used to determine the calibration functions f_i and g_i by fitting the experimental data to the values given by Equations 26 and 27. For both PSBAs the measured beam radii agree well with the calculated ones. A comparison of Figs 7 and 8 has already shown that Equation 24 holds in a very good approximation. This means that quadratic correction is sufficient by setting $f_2(\Delta)$ to zero in Equation 26. Furthermore, within the experimental errors no correction of the beam radius is necessary for PSBA 2 if the slit width 2Δ is chosen larger than 0.2 mm. In all experiments with PSBA 2, therefore, we did not correct the beam radius.

Correction of the divergence is more complicated. To get more information it was necessary to measure the divergence $(\theta/2)_{\mathrm{PSBA}}$ for a variety of input divergences $\theta/2$. For PSBA 1 this was accomplished by focusing the HeNe beam onto the entrance slit with different focusing lenses; for PSBA 2 the YAG laser was driven at different pumping powers. For the stable resonator used the varying refractive power is linked to a corresponding variation of mode order and divergence. In addition, for both PSBAs the 'real' divergence of the input field was measured in the focal plane of a lens. The results of this measurement are shown in Fig. 10. For PSBA 1 the measured curves can be explained very well by setting $g_2(\Delta) = 0$ and calculating $g_1(\Delta)$ with the experimental data in Fig. 9. For angles of divergence larger than 1.5 mrad it is even possible to neglect any correction. For PSBA 2 the dependence is totally different. It is apparent that the divergences measured with the PSBA are shifted with respect to the real ones. Equation 27 becomes applicable if $g_1(\Delta)$ is set to zero. The remaining shift function $g_2(\Delta)$ can now be determined from Fig. 10 by interpolation, as indicated by the broken lines, or by using the shifts in the lower

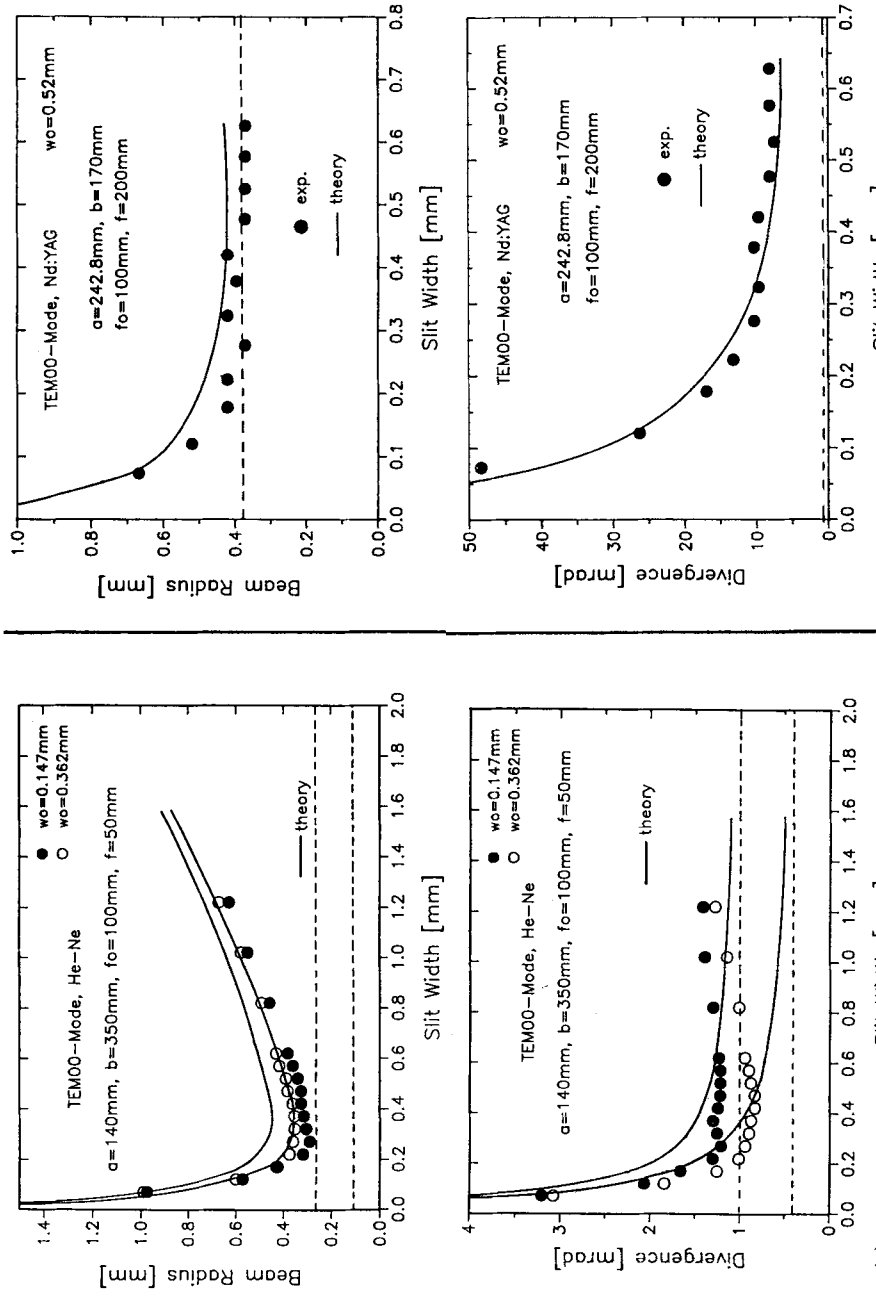

Figure 9 Measured beam radii $(d/2)_{PSBA}$ and angles of divergence $(\theta/2)_{PSBA}$ for Gaussian beams with beam waists located in plane 1 for the two PSBAs used in comparison with numerical solutions of the Fresnel integral equations (14) to (16) and Equations 19 and 20. The dependence on the silt width 2Δ of slit 2 is shown. The broken lines indicate real beam radius and divergence of the input field according to Equations 5 and 6. (a) PSBA 1: TEM_{00} mode, HeNe; $a = 140\,mm$, $b = 350\,mm$, $f_0 = 100\,mm$, $f = 50\,mm$, $\lambda = 0.6328\,\mu m$, $s = 25\,\mu m$. (b) PSBA 2: TEM_{00} mode, Nd:YAG; $a = 242.8\,mm$, $b = 170\,mm$, $f_0 = 100\,mm$, $f = 200\,mm$, $\lambda = 1.064\,\mu m$, $s = 25\,\mu m$.

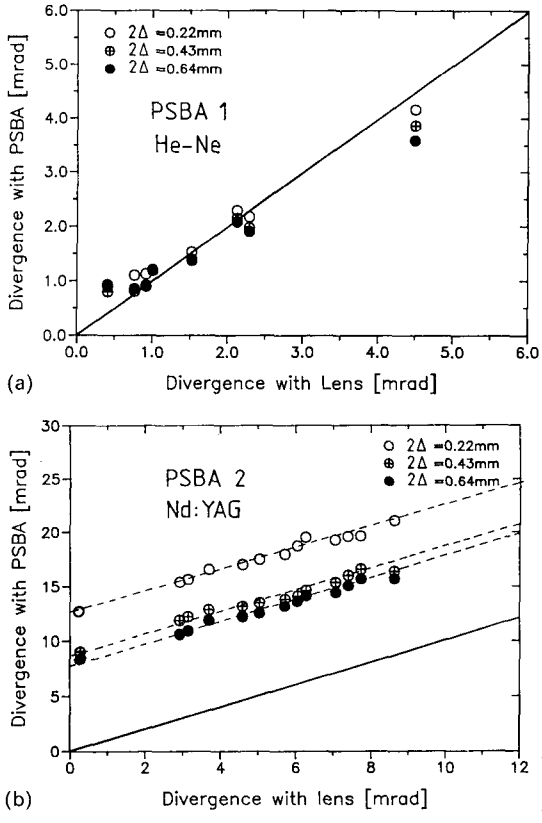

Figure 10 Measured angles of divergence $(\theta/2)_{PSBA}$ for the two PSBAs plotted versus the measured angles of divergence $(\theta/2)$. For PSBA 1 a HeNe Gaussian beam, for PSBA 2 multimode beams from a high power Nd:YAG laser were used. These curves can be used to calibrate the PSBA. (a) PSBA 1: a = 140 mm, b = 350 mm, f_0 = 100 mm, f = 50 mm, λ = 0.6328 μm, s = 25 μm. (b) PSBA 2: a = 242.8 mm, b = 170 mm, f_0 = 100 mm, f = 200 mm, λ = 1.064 μm, s = 25 μm.

right-hand curve of Fig. 9. After both systems were calibrated they were used to investigate the beam propagation of different laser beams.

5.3. Application

Before applying the PSBA to specific problems we first checked the applicability of the numerical solutions of Equations 14 to 16. Figure 11 shows a comparison of the calculated and recorded intensity distributions on plane 4 for the HeNe laser beam with its waist located on the entrance slit and with radius w_0 = 0.362 mm. With increasing width of slit 2, the ellipse starts rotating into a horizontal position and the same behaviour can be observed in the calculations.

It is more interesting of course, to track the HeNe beam in optical systems where a considerable change of beam parameters is provided. We placed the PSBA at a fixed distance of 1.2 m behind the beam waist and shifted a 200-mm lens located between. The set-up of the experiment and the results are presented in Fig. 12. The corrected beam radius is in good agreement with the theoretical curve obtained by solving the *ABCD* law for the q-parameter. Near the focal point the measured radius $(d/2)_{PSBA}$ is in the same order of magnitude as the term $\sqrt{[f_1(\Delta)]}$ (see Equation 26 with $f_2(\Delta) = 0$) and the errors caused by the correction are too high for accurate prediction of the beam radii. Nevertheless, for beam

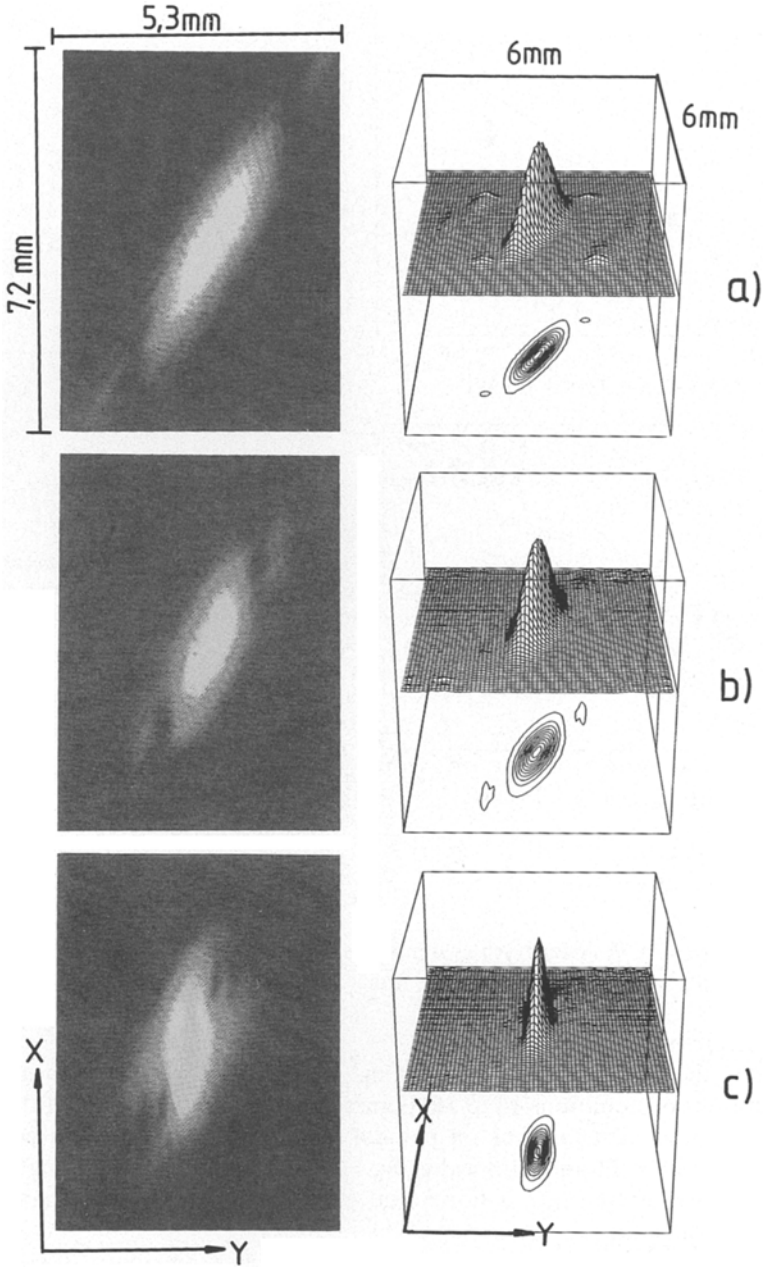

Figure 11 Comparison of measured and photographed intensity distributions of a Gaussian beam in the observation plane of PSBA 1 for three different slit widths 2Δ (a = 140 mm, b = 350 mm, f_0 = 100 mm, f = 50 mm, λ = 0.6328 μm, s = 25 μm): (a) Δ = 0.05 mm, (b) Δ = 0.1 mm, (c) Δ = 0.2 mm.

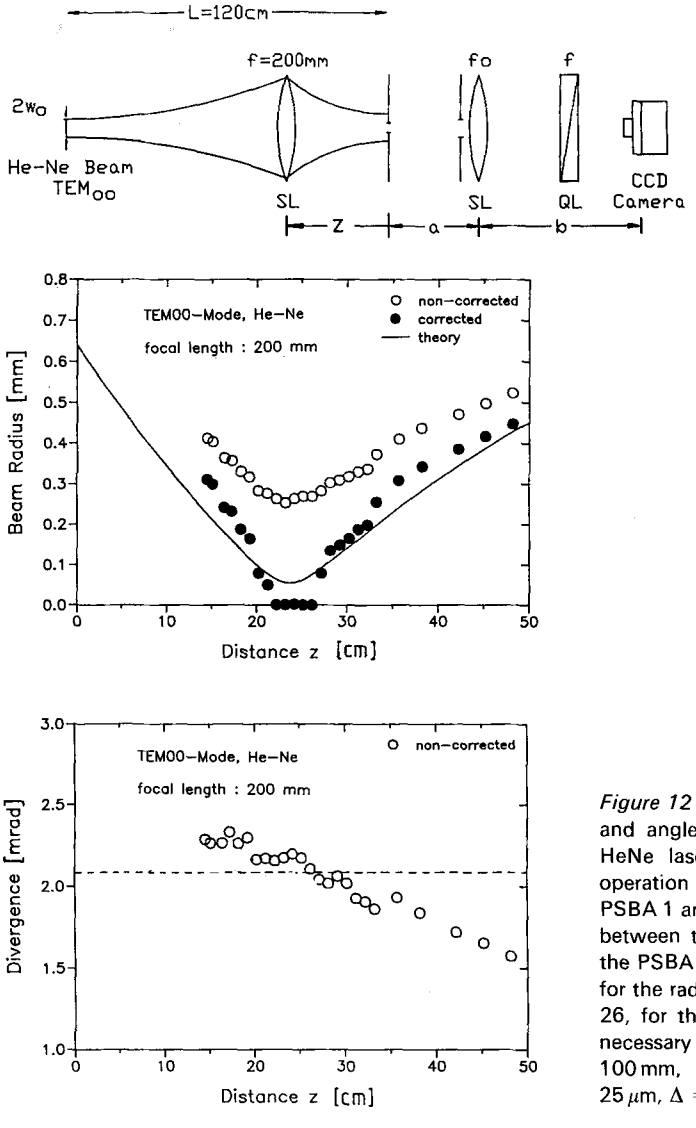

Figure 12 Measured beam radii $(d/2)_{PSBA}$ and angles of divergence $(\theta/2)_{PSBA}$ for a HeNe laser beam in fundamental mode operation with a 200-mm lens between PSBA 1 and the beam waist. The distance z between the lens and the entrance slit of the PSBA was varied. The corrected values for the radius were obtained with Equation 26, for the divergence no correction was necessary (a = 140 mm, b = 350 mm, f_0 = 100 mm, f = 50 mm, λ = 0.6328 μm, s = 25 μm, Δ = 0.11 mm).

radii not too small the corrected values can be used to determine the caustic of the beam. The measured divergence is correct also, as comparison with the theoretical angle related to the minimum spot size indicates. It was fascinating to look at the intensity profile in phase space in the course of this experiment. Since the radius of curvature R of the Gaussian beam changes with the distance z, the phase space ellipse is rotated as already discussed. Photographs taken in plane 4 for three different distances z are shown in Fig. 13 for the experiment presented in Fig. 12. It is worth noting that the ellipse does not stand upright when the beam waist is reached, which is contrary to the geometrical calculations presented in Fig. 2. This rotation is only caused by diffraction at slit 2.

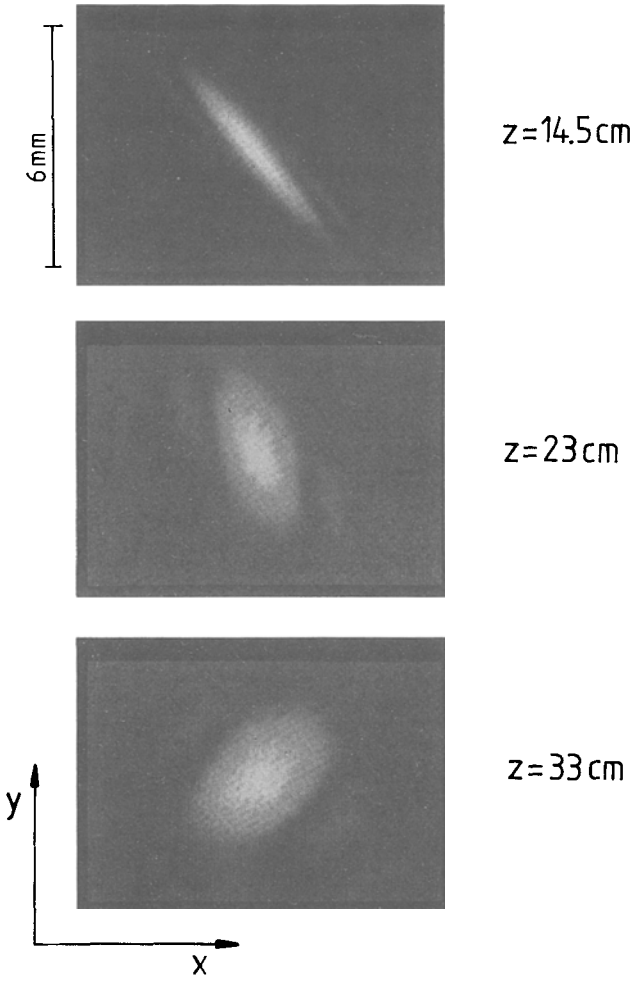

Figure 13 Photographs of the intensity distribution in the observation plane for different distances z for the experiment with the moving lens described in Fig. 12 (a = 140 mm, b = 350 mm, f_0 = 100 mm, f = 50 mm, λ = 0.6328 μm, s = 25 μm, Δ = 0.11 mm).

The most interesting application of the phase space beam analyser is the determination of the beam parameter product of a laser beam, especially when the beam quality strongly depends on the pumping conditions. We performed these experiments with the Nd : YAG laser and PSBA 2. To give the reader an idea what the distributions in the observation plane look like, photographs are presented in Fig. 14 for a fundamental mode and a high-order mode and two different widths of slit 2. As an example for a resonator with changing beam parameter product we used a nonsymmetric flat–flat resonator and increased the repetition rate. In this resonator the beam waist is always located on the output coupling mirror and imaging the waist onto the entrance slit of the PSBA can be accomplished with a fixed lens. The beam waist radii and the angles of divergence were calculated by using the *ABCD*

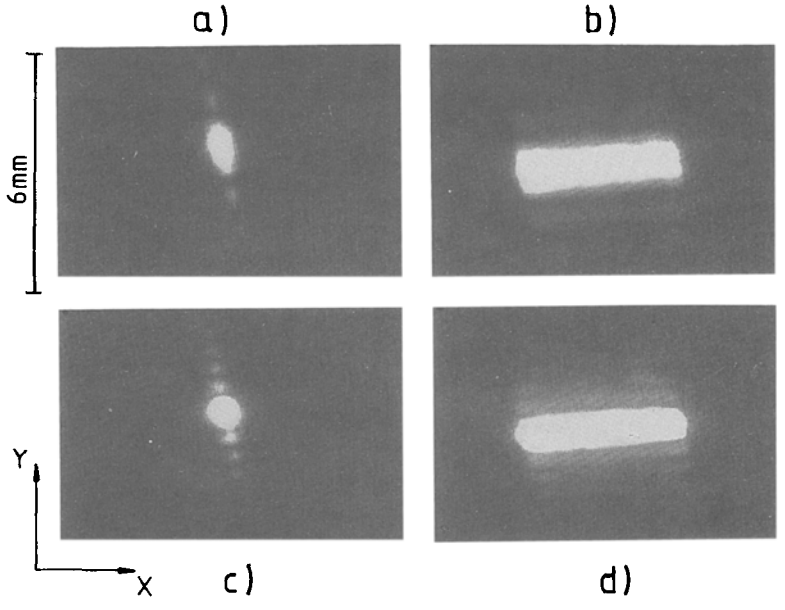

Figure 14 Photographs of intensity distributions in the observation plane of PSBA 2 for a YAG laser in fundamental mode operation and in multimode operation with 80 times diffraction-limited beam quality (a = 242.8 mm, b = 170 mm, f_0 = 100 mm, f = 200 mm, λ = 1.064 μm, s = 25 μm). (a) Δ = 0.1 mm, fundamental mode, w_0 = 0.52 mm. (b) Δ = 0.1 mm, multimode operation, beam radius 4.1 mm. (c) Δ = 0.2 mm, fundamental mode, w_0 = 0.52 mm. (d) Δ = 0.2 mm, multimode operation, beam radius 4.1 mm.

propagation rules for Gaussian beams and additionally measured with the common two-lens technique, before PSBA 2 was used. The set-up of the experiment and a comparison of the two measurements and the calculation are shown in Fig. 15. In Section 5.2 it was mentioned that a correction of the beam radius $(d/2)_{\mathrm{PSBA}}$ is not necessary and the angles of divergence must simply be shifted. After correction we see a perfect agreement with the values measured with the lenses. At 24 Hz repetition rate, which corresponds to a pumping power of 7.5 kW, the resonator goes unstable. In this case the field distribution on the output coupling mirror no longer has a planar wavefront, which means that the beam waist is located somewhere inside the resonator. Since the intensity distribution in the observation plane strongly depends on the radius of curvature of the phase distribution, the change from stable to unstable resonator can be well observed in phase space. Figure 16 shows photographs for repetition rates of 10, 23, 24 and 25 Hz, clearly indicating the sudden change of the phase space structure when the resonator goes unstable. This sensitivity against the phase radius R beats any common lens technique for observing changes in mode structure.

Finally, we used PSBA 2 to measure the focusing properties of a beam emerging from an unstable resonator with an output coupling mirror with hard aperture. A confocal resonator with magnification M = 3 and an aperture radius of 1.4 mm was used to measure beam radius and divergence in the vicinity of the focal spot as shown in Fig. 17. Again the correct beam parameter product of 1.4 mm mrad is obtained. Similarly to the stable modes, the structure in phase space rotates and outside the focal plane a double stripe structure appears due to the near-field being an annular ring with inner radius 1.4 mm and outer radius 4 mm (Fig. 18).

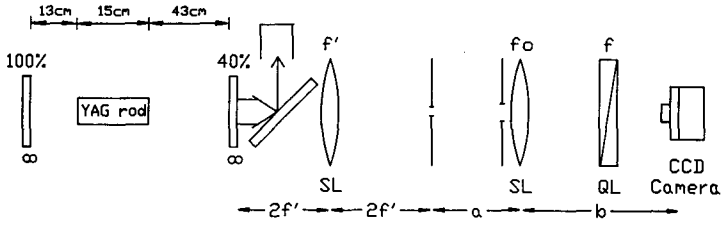

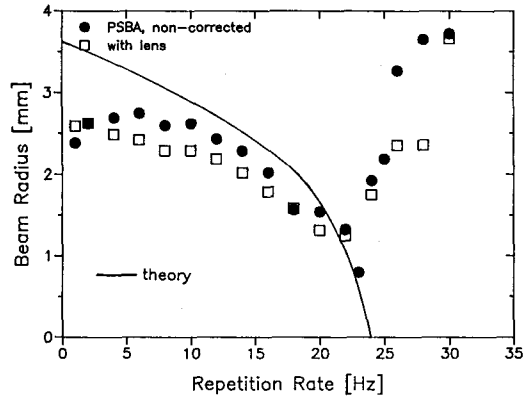

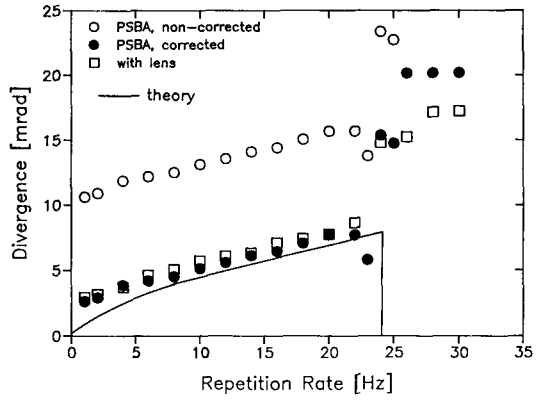

Figure 15 Beam radii $(d/2)_{PSBA}$ and angles of divergence $(\theta/2)_{PSBA}$ measured with PSBA 2 for a pulsed Nd:YAG laser with flat–flat resonator (a = 242.8 mm, b = 170 mm, f_0 = 100 mm, f = 200 mm, $2s$ = 50 μm, 2Δ = 0.43). The corrected values are compared with the results obtained by measuring beam radius and divergence with a lens and with the theoretical curves given by matrix optics and Gaussian beam propagation rules.

In summary, the experiments described above performed with different laser beams and two PSBAs clearly demonstrate that this optical device is very useful for the determination of beam parameters and, in addition, the sensitivity against phase alterations makes it a powerful tool for looking at changes in mode and phase structure of resonator modes.

6. Conclusion

The properties of the phase space beam analyser were investigated theoretically by solving the corresponding Fresnel integrals and this indicated that correction of the diffraction

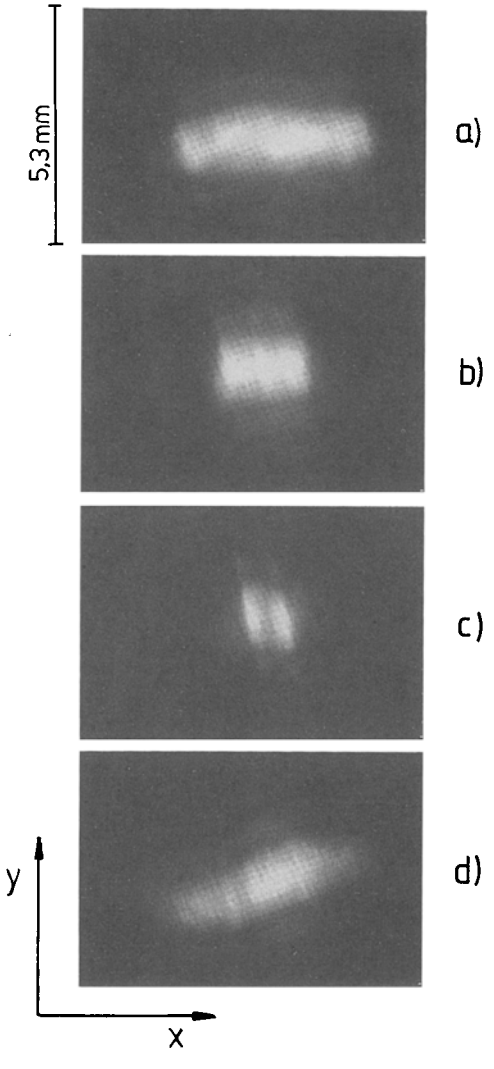

Figure 16 Photographs of the intensity distributions taken in the observation plane of PSBA 2 at different repetition rates for the curves presented in Fig. 15. The shape suddenly changes when the resonator goes unstable. This is due to the changing radius of curvature R of the phase front and the increasing beam size. (a) 10 Hz; (b) 23 Hz; (c) 24 Hz; (d) 25 Hz.

effects is possible. This calibration can be performed theoretically or by using input beams with known divergences and radii. Two PSBAs were calibrated with Gaussian beams and applied to different beam-propagation problems. The results clearly verified the applicability of the PSBA to the determination of beam parameter products and beam caustics as well as its ability to provide more insight into mode properties of resonators. The two PSBAs used were chosen by the cylindrical lenses we had rather than by a detailed optimization according to Equations 24 and 25. In the future we will focus our attention on a further increase of angular and spatial resolution.

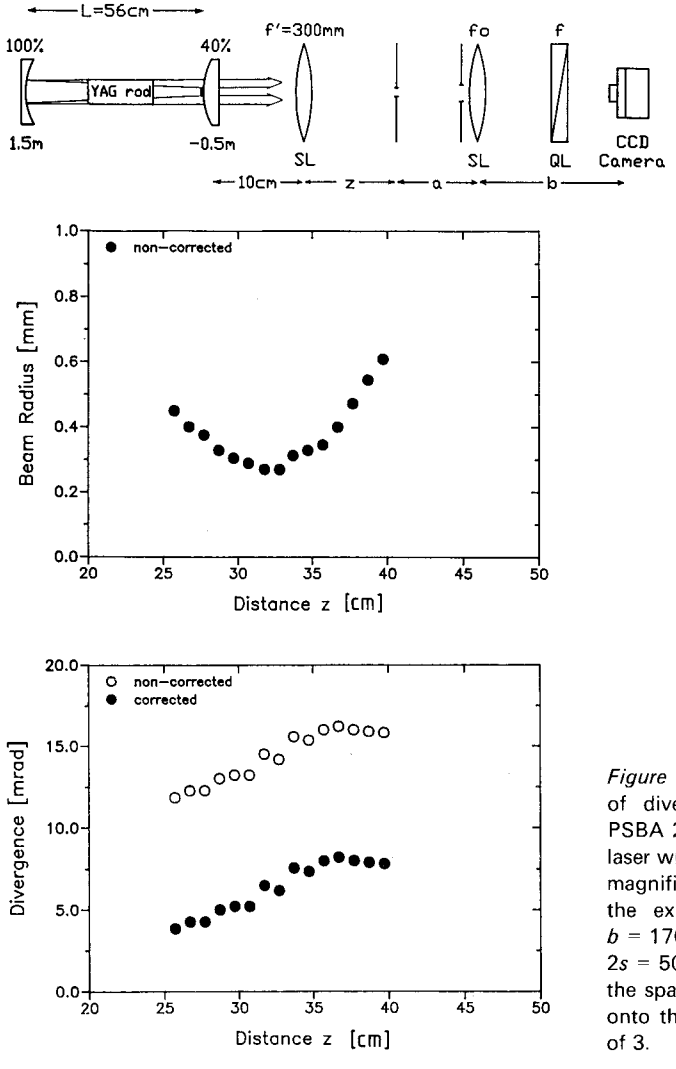

Figure 17 Beam radii $(d/2)_{PSBA}$ and angles of divergence $(\theta/2)_{PSBA}$ measured with PSBA 2 for a focused beam of a Nd:YAG laser with confocal unstable resonator with magnification 3. The upper graph presents the experimental set-up (a = 242.8 mm, b = 170 mm, f_0 = 100 mm, f = 200 mm, $2s$ = 50 μm, 2Δ = 0.43 mm). To increase the spatial resolution, plane 4 was imaged onto the CCD chip magnified by a factor of 3.

Acknowledgement

We are grateful to Walther Goethals from Lumonics Ltd, Rugby, UK, for very helpful discussions and for supplying a -25 mm cylindrical lens. This work was supported by the German Ministry of Research and Technology (BMFT) under contract 13N5531.

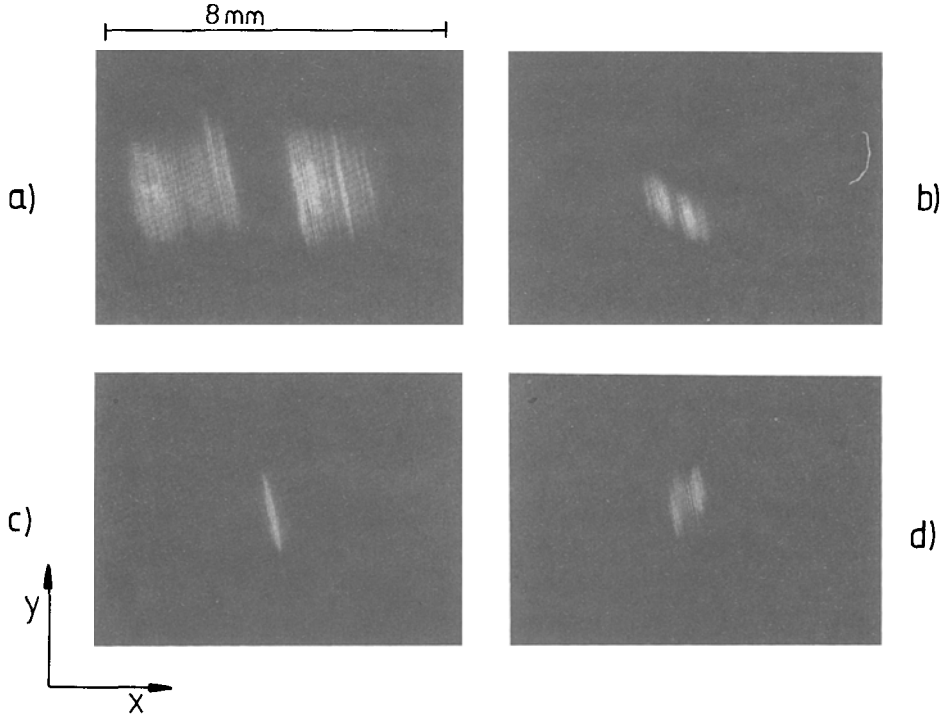

Figure 18 Photographs of the intensity distributions in plane 4 taken at different distances z from the lens in the experiment described in Fig. 17. (a) z = 0 cm; (b) z = 25.7 cm; (c) z = 32.7 cm; (d) z = 38.7 cm.

References

1. G. NEMES, I. E. TEODORESCU and M. NEMES, *Proc. 3rd International School of Coherent Optics* edited by I. Ursu, A. M. Prokhorov (CIP Press, Bucharest 1983), Part I.
2. R. SIMON and N. MUKUNDA, E. L. G. SUDARSHAN, *Opt. Commun.* **65** (1988) 322.
3. P.A. BELANGER, *Opt. Lett.* **16** (1991) 196.
4. W. A. E. GOETHALS, Geometrical optics of laser beams, *Physics and Technology of Laser Resonators*, edited by D. R. Hall and P. E. Jackson (Adam Hilger, Bristol, 1989) p. 143.
5. R. SIMON, E. C. G. SUDARSHAN and N. MUKUNDA, *Phys. Rev. A* **29** (1984) 3273.
6. H. WEBER, *J. Mod. Opt.* **39** (1992) 543.
7. S. A. COLLINS, *J. Opt. Soc. Am.* **60** (1970) 1168.
8. H. KOGELNIK and T. LI, *Proc. IEEE* **5** (1966) 1312.
9. L. QUIANG, W. SHAOMIN, J. ALDA and E. BERNABEU, *Optik* **85** (1990) 67.